The FEBS Journal

FEBS PRESS science publishing by scientists

Arabidopsis thaliana Hcc1 is a Sco-like metallochaperone for Cu_A assembly in Cytochrome *c* Oxidase

María-Eugenia Llases[1], María-Natalia Lisa[1,2], Marcos N. Morgada[1,3], Estefanía Giannini[1], Pedro M. Alzari[4] and Alejandro J. Vila[1,2,3]

1 Instituto de Biología Molecular y Celular de Rosario (IBR CONICET-UNR), Rosario, Argentina
2 Plataforma de Biología Estructural y Metabolómica (PLABEM), Rosario, Argentina
3 Area Biofísica, Departamento de Química Biológica, Facultad de Ciencias Bioquímicas y Farmacéuticas, Universidad Nacional de Rosario, Argentina
4 Unité de Microbiologie Structurale, Institut Pasteur, Université Paris Diderot, Paris, France

Keywords
copper; Cu_A; Cytochrome-*c*-Oxidase; metallochaperone; Sco

Correspondence
A. J. Vila, Instituto de Biología Molecular y Celular de Rosario (IBR, CONICET-UNR), Ocampo y Esmeralda, Rosario, S2002LRK, Argentina
Tel: +54 3414237070, ext: 632
E-mail: vila@ibr-conicet.gov.ar
Website: http://www.ibr-conicet.gov.ar/laboratorios/vila

(Received 30 May 2019, revised 3 July 2019, accepted 22 July 2019)

doi:10.1111/febs.15016

The assembly of the Cu_A site in Cytochrome *c* Oxidase (COX) is a critical step for aerobic respiration in COX-dependent organisms. Several gene products have been associated with the assembly of this copper site, the most conserved of them belonging to the Sco family of proteins, which have been shown to perform different roles in different organisms. Plants express two orthologs of Sco proteins: Hcc1 and Hcc2. Hcc1 is known to be essential for plant development and for COX maturation, but its precise function has not been addressed until now. Here, we report the biochemical, structural and functional characterization of *Arabidopsis thaliana* Hcc1 protein (here renamed Sco1). We solved the crystal structure of the Cu^{+1}-bound soluble domain of this protein, revealing a tri coordinated environment involving a $CxxxCx_nH$ motif. We show that *At*Sco1 is able to work as a copper metallochaperone, inserting two Cu^{+1} ions into the Cu_A site in a model of CoxII. We also show that *At*Sco1 does not act as a thiol-disulfide oxido-reductase. Overall, this information sheds new light on the biochemistry of Sco proteins, highlighting the diversity of functions among them despite their high structural similarities.

Database
PDB entry 6N5U (Crystal structure of *Arabidopsis thaliana* ScoI with copper bound).

Introduction

COX is the heme/copper terminal oxidase of the respiratory chain in most aerobic organisms. COX is a multimeric complex (Fig. 1) with three conserved subunits (CoxI, CoxII and CoxIII) that contain four cofactors essential for its function (two heme moieties and two copper centers: Cu_A and Cu_B) [1]. The assembly of the oxidase is a complex process involving the synthesis and folding of the individual subunits and the incorporation of the metal cofactors. Maturation of the two copper sites is a fundamental step in the assembly of human oxidase and requires at least seven genes, a fact that highlights the intrinsic complexity of the biosynthesis of the oxidase [2–4].

Copper is an essential micronutrient for all living organisms, as it is employed as a catalytic cofactor in COX, among many other metalloenzymes [5–8]. Due to its coordination properties and its two easily accessible oxidation states (Cu^{+1} and Cu^{+2}), copper enzymes

Abbreviations
Bcs, bathocuproine disulfonate; COX, cytochrome *c* oxidase; EXAFS, Extended X-ray absorption fine structure; HSQC, heteronuclear single quantum coherence; ICP-MS, Inductively coupled plasma mass spectrometry; IMS, intermembrane space; LMCT, ligand to metal charge transfer; PAR, 4-(2-pyridilazo)-resorcinol; RMSD, Root-mean-square deviation of atomic positions.

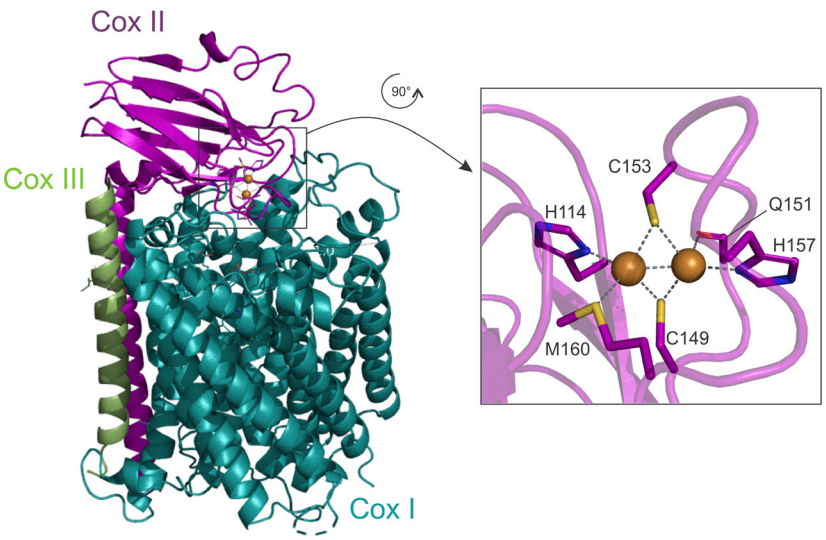

Fig. 1. Crystal structure of the COX ba_3 complex from *Thermus thermophilus* (PDB ID 1EHK). Inset: the Cu_A center in CoxII soluble domain. Copper ligands are shown in stick representation and copper atoms are depicted by brown spheres.

are efficient catalysts in many redox reactions. However, this reactivity also makes copper toxic. Dysregulation of the copper levels may elicit unwanted redox reactions and the production of reactive oxygen species (ROS) [9]. In addition, Cu^{+2} is at the top of the Irwin-Williams series, being able to tightly bind to adventitious metal binding sites in proteins, outcompeting the native metal ions and consequently inactivating these proteins [10].

To deal with these potential hazards, cells have developed different mechanisms to regulate intracellular copper levels [11–14]. These mechanisms include copper uptake, translocation [15], transport and storage by a complex protein network that avoids accumulation of free copper ions in cells [16,17], finally ensuring their correct insertion in the active sites of target proteins through the action of metallochaperones [18].

Cu_A is the electron entry port of COX, located in the soluble domain of CoxII. The structure of the Cu_A site from the *Thermus thermophilus* oxidase is shown in Fig. 1. This site is composed by two copper ions bridged by the sulfur atoms of two cysteine residues, constituting a rigid core able to exchange one electron and cycle between the oxidation states $Cu^{+1}Cu^{+1}$ and $Cu^{+1.5}Cu^{+1.5}$ [19–21]. The metal center is further stabilized by four extra ligands: two equatorial histidines together with a methionine residue and a backbone carbonyl moiety in axial positions (Fig. 1, inset). Defects in the assembly of this copper site lead to a non-functional oxidase and have lethal effects in organisms lacking an alternative oxidase [22–25]. Thus, the proper assembly of the Cu_A site is essential for aerobic respiration [3].

The soluble domain of CoxII is located in oxidizing environments: the intermembrane space (IMS) in mitochondria or the extra-cytoplasmic space in bacteria [26–29]. As a consequence, the proper assembly of Cu_A requires two functions: (a) a specific metallochaperone located in the same cellular compartment that inserts the copper ions in the oxidase, and (b) a thiol-reductase that maintains the thiol residues of the cysteine ligands in the reduced state, enabling copper binding. These functions have been attributed in most cases to proteins from the Sco (named after Synthesis of Cytochrome oxidase) family, that are present in all organisms expressing a heme-copper oxidase [30]. Sco proteins are anchored to the inner mitochondrial membrane through a transmembrane helix, with a soluble globular domain located in the IMS, the same cellular localization of CoxII. The function of Sco proteins has been attributed to the soluble domain, which is characterized by a thioredoxin/peroxiredoxin-like fold but, in contrast to thioredoxins, Sco proteins can bind copper ions [31]. This metal binding ability is given by two cysteine residues located in a CxxxC motif, with an additional β-hairpin containing a histidine residue that completes the copper coordination sphere. Since this hairpin is absent in thioredoxins, it is known as the Sco loop [32,33]. Sco proteins are conserved in nearly all aerobic organisms and are involved in the assembly of the Cu_A site [30,34]. However, their precise role and the number of essential Sco orthologs differ among organisms. Indeed, Sco proteins can act as thiol-oxidoreductases and/or copper chaperones, depending on the organism [35–37], and their function can be complemented by other periplasmic or mitochondrial proteins.Due to this functional versatility, the biochemical

roles of Sco proteins in Cu_A assembly can be only addressed by *in vitro* experiments with purified proteins [35–37]. Recently the mechanism of assembly of the human mitochondrial Cu_A has been elucidated by using an *in vitro* approach. It was shown that two Sco orthologs are required for the assembly of the center: Sco2 acts as a thiol-reductase while Sco1 acts as a metallochaperone [36].

Arabidopsis thaliana expresses two Sco homologs: Hcc1 and Hcc2 (called after *homolog of copper chaperone*) [38]. Hcc1 is essential for COX activity and plant viability, whereas Hcc2 lacks the canonical $CxxxCx_nH$ motif and its involvement in COX maturation is not clear [39,40]. This reveals that plant mitochondria express a different set of Sco orthologs compared to mammalian mitochondria, where two essential Sco-like proteins display complementary functions in Cu_A assembly [24,36]. The lack of one essential ortholog in plants with respect to human mitochondria, indicates that either one of the functions attributed to human Sco proteins is dispensable in plant cell, or that Hcc1 can perform both. We therefore decided to analyze the structure and precise function of Hcc1, with the aim of expanding the available knowledge on the extent of conservation of Sco structure and function in eukaryotes and providing new insights on the mechanisms that different cells have evolved to guarantee the proper assembly of a vital center as Cu_A.

Here we report the biochemical, structural and functional characterization of Hcc1. We show that this protein is an efficient copper metallochaperone for CoxII, confirming the structural and functional similarity with other eukaryotic Sco proteins. This evidence highlights the diversity of biochemical properties of Sco proteins, triggering new questions about the structural features that determine their different reactivity.

Results

Arabidopsis thaliana Hcc1 is a copper binding protein

Sco proteins contain a mitochondrial targeting sequence, a helical membrane anchoring fragment and a soluble domain. Since the essential features for metal binding and redox reactivity are present in the soluble domain, biochemical and biophysical studies on this fragment have been exploited to obtain a *bona fide* description of the protein function [35–37,41]. We worked here with the C-terminal 165 residues of Hcc1 based on previous studies with the homologous proteins in bacteria (170 residues) [35], yeast (200 residues) [23] and mammals (165 residues) [34].

The soluble domain of Hcc1 was expressed and purified in the apo form, i.e., with no metal bound. The reduced form (with cysteine residues as free thiols) of this variant was later incubated with excess Cu^{+1} or Cu^{+2} under anaerobic conditions. ICP-MS (Inductively Coupled Plasma Mass Spectrometry) measurements after removal of excess metal ions indicated the binding of one equivalent of either Cu^{+1} or Cu^{+2} to Hcc1. ICP-MS did not reveal the presence of other transition metal ion to significant levels.

Cu^{+2}-Hcc1 was orange, as previously reported for other Cu^{+2}-Sco proteins (from human, yeast, *T. thermophilus* and *Bacillus subtilis*) [35,42,43]. The electronic absorption spectrum of Cu^{+2}-Hcc1 was dominated by a strong feature centered at 362 nm, assigned to Cys-Cu^{2+} ligand-to-metal-charge transfer (LMCT) transitions (Fig. 2) by analogy to the spectral data for Cu^{2+}-nitrosocyanin [44], and additional ligand field bands in the visible region [45].

The crystal structure of Cu-bound Hcc1

The copper-loaded soluble domain of Hcc1 crystallized under aerobic conditions in the space group $P2_1$ (Table 1). X-ray diffraction data were phased by molecular replacement and the crystal structure was refined to 2.66 Å. The final atomic model contains three equivalent copies of Hcc1 in the asymmetric unit, with an average root-mean-square deviation of atomic positions (RMSD) value of 0.1 Å among 157 alpha-carbons in pairwise comparisons. The structure was deposited in the PDB database with accession number 6N5U.

Hcc1 adopted a typical Sco fold, i.e., a thioredoxin/peroxiredoxin fold with four alpha helixes and nine beta strands (Fig. 3A), comparable to the Sco variants from human (PDB ID 2GGT, [34]), yeast (PDB ID

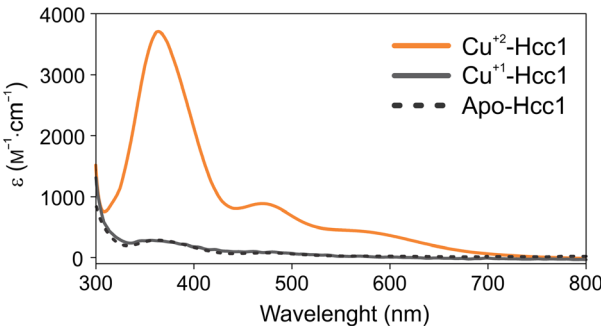

Fig. 2. UV-Vis absorption spectrum of apo-Hcc1 (dotted black line), Cu^{+2}-Hcc1 (solid orange line) and Cu^{+1}-Hcc1 (solid grey line). All spectra were recorded in 50 mm phosphate buffer, 200 mm NaCl, at pH 7.

Table 1. Data collection and refinement statistics.

*At*Sco1 (PDB ID 6N5U)	
Data collection	
Space group	$P2_1$
Cell dimensions	
a, *b*, *c* (Å)	53.65, 80.44, 72.31
α, β, γ (°)	90.00, 94.75, 90.00
Resolution (Å)	44.75–2.66 (2.79–2.66)[a]
R_{merge}	0.068 (0.327)
$I/\sigma I$	5.7 (1.5)
CC(1/2)	0.996 (0.932)
Completeness (%)	99.0 (99.6)
Redundancy	2.9 (2.9)
Refinement	
Resolution (Å)	44.75–2.66 (2.82–2.66)
No. reflections	17 534 (2848)
R_{work}/R_{free}	18.7/23.3
No. atoms	
Protein	3859
Cu^{+1}	3
Water	90
B-factors	
Protein	55.39
Cu^{+1}	52.66
Water	37.49
R.m.s. deviations	
Bond lengths (Å)	0.01
Bond angles (°)	1.14

[a] One protein crystal was employed for structure determination. Values in parentheses are for highest-resolution shell.

2B7J, [46]), and *Bradyrhizobium japonicum* (PDB ID 4WBR for the copper bound species and 4WBJ for the apo form), with RMSD values within the range 0.78–1.05 Å (Fig. 3C–E). The comparison of Hcc1 and *B. subtilis* Sco (PDB ID 1XZ0, [41]) revealed a higher RMSD (1.62 Å), mainly due to divergent conformations of the Sco loop and the cysteine-containing motif in the latter (Fig. 3F).

The characteristic Sco loop, comprising Hcc1 residues 117–131 (see the Experimental procedures for details on the numbering scheme used in this work), is fully defined in two of the three protein molecules in the asymmetric unit. For all monomers, additional electron density was evident at the base of the Sco loop, i.e. the canonical copper-binding site in Sco proteins. This feature was interpreted as a bound copper ion, consistent with the measured protein:metal stoichiometry. The copper ion is coordinated by the S_γ atoms of C42 (d~2.4 Å) and C46 (d~2.3 Å) (from loop L3) and the N_ε atom from H131 (d~2.5 Å) (at the base of the Sco loop) (Fig. 3B). The coordination sphere of the metal ion adopts a distorted trigonal planar geometry, with the copper atom located 0.4 Å outside of the plane defined by the three protein ligands. No evidence of a fourth metal ligand was found for any of the three molecules in the asymmetric unit of the crystal structure. Only for one of the molecules, a positive peak of electron density compatible with a water molecule was found at a distance of 4.4 Å from the metal ion, which cannot be interpreted as a bonding interaction. The observed trigonal-planar distorted geometry is consistent with a Cu^{+1} ion, despite the fact that crystal growth took place under aerobic conditions. This can be attributed to photoreduction of the metal ion, a common and well documented process that occurs upon high-power synchrotron irradiation of copper proteins [47,48]. Overall, this structure allows us to describe Hcc1 as *A. thaliana* Sco (*At*Sco1).

Engineering a soluble variant of *Arabidopsis thaliana* CoxII

The *in-vitro* biochemical study of the function of Sco proteins in Cu_A assembly has been challenging due to the difficulty in purifying the Cu_A-containing CoxII subunit in a soluble and stable form. This has been achieved for the CoxII subunits of the bacterial oxidases from *B. japonicum* [37], *B. subtilis* [49], *P. denitrificans* [50] and *T. thermophilus* [51]. However, there are no reports of stable eukaryotic soluble domain of CoxII. Eukaryotic oxidases are much more complex than the bacterial ones, with CoxII showing hydrophobic interactions with other subunits, without contact with the solvent (Fig. 4A–C). As a result, eukaryotic CoxII domains are highly unstable in solution.

All known CoxII subunits are characterized by a cupredoxin fold [52], with eight β strands forming a Greek key β-barrel, where the copper binding site is defined by three loops (Fig. 4D) [27,29,53]. In spite of the lack of crystal structures for plant heme/copper oxidases, *Arabidopsis thaliana* CoxII is predicted to hold the same fold, based on its homology to other CoxII subunits (Fig. 4E and F). Figure 4E shows the 3D structure of the soluble CoxII subunit from *T. thermophilus* ba_3 oxidase superimposed to the predicted structure of *A. thaliana* CoxII, generated by the Robetta server (http://robetta.bakerlab.org/).

The three loops located at the top of the β-barrel provide the copper ligands and the putative recognition patch for metallochaperones in the non-metallated form [54–56]. The length of these three loops is the same among all oxidases, and the metal ligands are conserved (Fig. 4D,E). Since the CoxII subunit from *A. thaliana* is expected to be unstable as its homologues, to probe the function of *At*Sco1, we designed a chimeric CoxII variant (CoxII**). The protein was

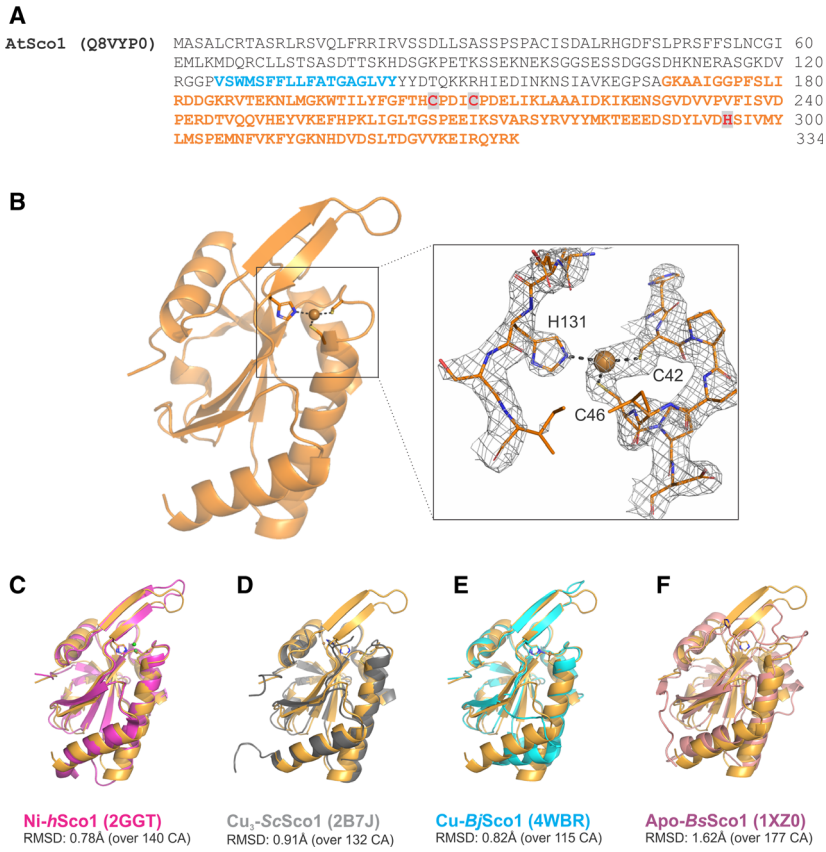

Fig. 3. (A) Sequence of the full Hcc1 protein (Uniprot ID code: Q8VYP0). The transmembrane domain is colored in cyan. The expressed sequence is colored in orange (residues 4 to 160, in the numbering of the desposited PDB structure). Crystal structure of Cu^{+1}-*At*Sco1: (B) Overall topology. The protein is depicted as orange ribbons. Metal ligands are highlighted in sticks. Highlight: The copper binding site. Protein residues are shown in sticks colored as follows: C in orange, N in blue, O in red and S in yellow. The 2mFo–DFc electron density is contoured to σ = 1.8 and represented as a gray mesh. The Cu^{+1} ion is shown as a brown sphere. Dashed lines represent bonding interactions. Comparison of Cu^{+1}-*At*Sco1 crystal structure (PDB ID 6N5U) with that of Sco variants reported in other works: (C) Ni-bound human Sco1 (PDB ID 2GGT), (D) Cu-bound *S. cerevisiae* Sco1 (PDB ID 2B7J), (E) Cu-bound *B. japonicum* Sco (PDB ID 4WBR) and (F) apo *Bacillus subtilis* Sco (PDB ID 1XZ0).

designed using the β-barrel of the *T. thermophilus* oxidase (which is highly stable in solution and easy to manipulate), and the three loops that surround the Cu_A site from from *A. thaliana* CoxII (Fig. 4G). This approach has already been used successfully to build a chimeric mimic of human CoxII [36].

Purified CoxII** is soluble and binds two copper ions forming a typical Cu_A center. The UV-Vis spectrum of the oxidized CoxII** Cu_A center resembled that of native Cu_A sites (Fig. 4H). Besides, it was possible to reduce the metal center in the chimera to the $Cu^{1+}Cu^{1+}$ form and then re-oxidize it back, validating CoxII** as a robust model to test the assembly of the Cu_A center.

Next, we recorded the $^{1}H,^{15}N$-HSQC spectra of ^{15}N-labeled CoxII** in all possible metallation/oxidation states, namely: (1) the apo state, with (a) reduced (apo-CoxII**$_{2SH}$) and (b) oxidized (apo-CoxII**$_{SS}$) cysteines, and (2) the metal-bound state, in the (a) reduced ($Cu^{1+}Cu^{1+}$-CoxII**) and (b) oxidized ($Cu^{1.5+}Cu^{1.5+}$-CoxII**) forms (Fig. 5). The $^{1}H,^{15}N$-HSQC spectra of the distinct states present different signatures that allow a direct identification of each species.

Triple resonance experiments on $^{15}N^{13}C$-$Cu^{1+}Cu^{1+}$-CoxII** samples allowed assignment of 103 out of 117 expected resonances (86%) in $^{1}H,^{15}N$-HSQC spectra. The spectral signature of this protein form is given by the crosspeaks corresponding to the amide moieties in the metal binding residues (Fig. 5). These resonances are broadened beyond the detection limit due to the proximity of the mixed-valence Cu_A paramagnetic center on the spectrum of $Cu^{1.5+}Cu^{1.5+}$-CoxII**. Also, 24 shifted crosspeaks were exclusive to this species, possibly corresponding to perturbed residues relatively far from the paramagnetic site. The $^{1}H,^{15}N$-HSQC spectra of the apo forms showed less crosspeaks than those of the Cu-bound forms (89 for apo-CoxII**$_{SS}$ and 104 for apo-CoxII**$_{2SH}$). The absence of the metal ions lead to line broadening due to a higher flexibility in the metal binding loops [54].

Thus, NMR provides a means for a straightforward identification and quantification of the relative amounts of the four possible CoxII** states. Therefore, next we used this technique to test the redox and metallochaperone activities of *At*Sco1 towards the chimera CoxII**.

Arabidopsis thaliana Sco1 is devoid of thiol-reductase activity

The thiol-reductase activity of the Sco proteins was originally suggested upon the report of the crystal

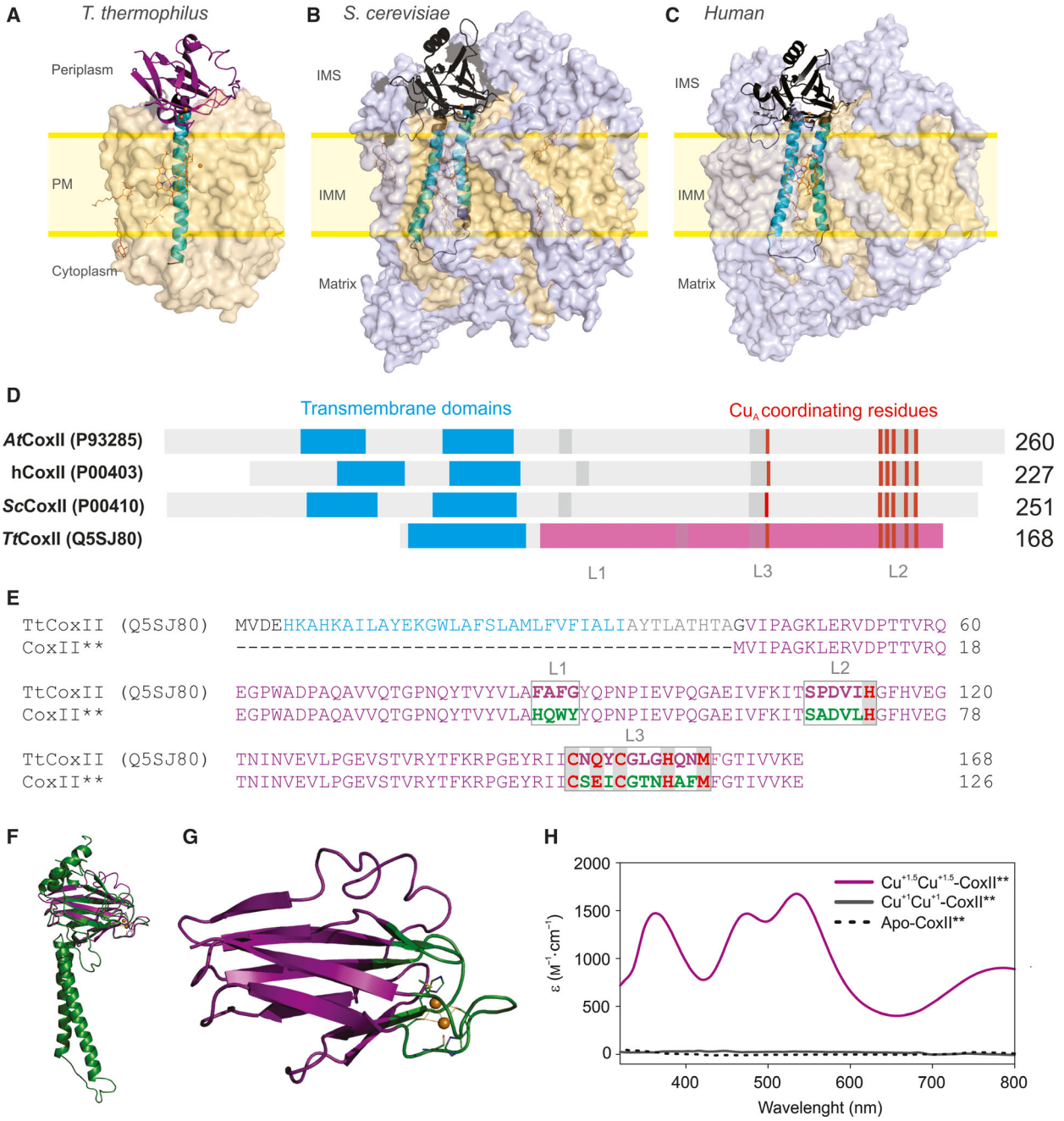

Fig. 4. (A–C) Structures of the COX complexes from: *Thermus thermophilus* (PDB ID 3EH5), *S. cerevisiae* (PDB ID 6HU9) and human (PDB ID 5XTH), respectively. The highly conserved subunits CoxI and CoxIII are depicted as light-orange surfaces. Accesory subunits, unique for eukaryotic complexes, are depicted as light-blue surfaces. (D) Structural features of CoxII variants from: *A. thaliana*, human, *S. cerevisiae* and *T. thermophilus*. Color scheme: transmembrane regions in cyan, conserved copper ligands in red, loops around the copper binding site in dark gray or purple on a light colored background. The soluble domains of eukaryotic CoxII variants are larger than for *Tt*CoxII, due to an insertion between loops L1 and L2 that is distant in the structure from the copper site. The region colored in purple corresponds to the expressed soluble construct. (E) Comparison between *T. thermophilus* CoxII and the expressed chimeric protein CoxII**. Color scheme is consistent with panel (A). (F) An homology model of *At*CoxII calculated by the Robetta server (http://robetta.bakerlab.org/) is shown in green superimposed to the crystal structure of the soluble fragment of *T. thermophilus* CoxII in purple. (G) *In silico* model of the chimera CoxII**. The color scheme highlights residues from *Tt*CoxII (purple) and *At*CoxII (green). (H) UV-Vis spectrum of $Cu^{1.5+}Cu^{1.5+}$- CoxII** (Solid purple line), $Cu^{1+}Cu^{1+}$- CoxII** (Solid gray line) and apo-CoxII** (Dotted black line) in 50 mM phosphate buffer, 200 mm NaCl, at pH 7.0.

structure of *B. subtilis* Sco disclosing the existence of a mixed redox form (Sco_{2SH} and Sco_{SS}) [41]. This redox activity was later demonstrated biochemically for the Sco protein from *T. thermophilus* [35,57], which is able to reduce the oxidized cysteine residues of CoxII from the same organism. A similar reactivity was reported for Cu^{+1}-bound human Sco2, while the apo variant of human Sco2 was devoid of this activity [36].

We therefore tested the thiol-reductase activity of apo-reduced Sco1 ($Sco1_{2SH}$). With this aim, we mixed ^{15}N-apo-CoxII**$_{SS}$ with unlabeled Sco_{2SH} at a 1:2 ratio in an NMR tube under anaerobic conditions. There were no changes in the HSQC spectrum after one day at room temperature, and no resonances corresponding to the apo-CoxII**$_{2SH}$ species appeared (data not shown).

We then investigated the possibility of a copper-dependent reduction by adding one equivalent of Cu^{+1}-Sco1 to ^{15}N-apo-CoxII**$_{SS}$. A set of 21 cross peaks characteristic of ^{15}N-apo-CoxII**$_{SS}$ disappeared, and 12 new resonances emerged. These 12 peaks did not correspond to any of the four CoxII** states previously characterized (Fig. 6A), suggesting the accumulation of an intermediate species. No further changes were evident in the reaction sample even after one day. No resonances corresponding to the ^{15}N-apo-CoxII**$_{2SH}$ were detected.

We then decided to address if this new species could correspond to an intermediate in a redox-coupled copper transfer. Addition of excess Cu^{+1}-Sco1 would allow the reaction to proceed towards the formation of a binuclear Cu_A formation given that the stoichiometry requires two equivalents of copper ions.

Addition of up to 3 equivalents of Cu^{+1}-Sco1 to oxidized CoxII** did not elicit changes in the spectra even after 24hs (data not shown). This indicates that Cu^{+1}-Sco1 is not able to perform copper transfer coupled to the reduction of disulfide bridges.

We conclude that under the studied conditions, Sco1 is not able to reduce the cystine bond of CoxII** neither in the apo nor in its metallated form.

Arabidopsis thaliana Sco1 is a metallochaperone

Finally, we tested the ability of Sco1 to deliver Cu^{+1} to the reduced form of apo-CoxII**. When 2 equivalents of unlabeled Cu^{+1}-Sco1 were added to ^{15}N-CoxII**$_{2SH}$, all the unique resonances from the apo form disappeared, giving rise to a spectrum that corresponds to the ^{15}N-$Cu^{1+}Cu^{1+}$-CoxII** form (Fig. 6B). This spectrum was indistinguishable from that obtained by reduction of $Cu^{1.5+}Cu^{1.5+}$-CoxII** with DTT and ascorbic acid (Fig. 5). These results are not consistent with the affinity constants for copper binding measured for the isolated proteins, suggesting the presence of other factors that govern copper transfer.

Resonances corresponding to the amide protons of the metal ligands in CoxII** were clearly observable in the spectra of the reaction mixture (Fig. 6B). The signals from C149 and C153, bridging the two copper ions were clearly observed. The peak corresponding to C153 showed a reduced intensity, also for a protein sample metallated by direct addition of copper ions, probably due to the higher exposure of this residue to the solvent. The peaks assigned to the other four ligands (H114, E154, H157 and M160) are also indicated. None of these peaks are present in the HSQC spectra of other states of CoxII**, indicating that copper insertion was successful. Comparison of the intensities of the resonances from the metal ligands with selected peaks distant from the metal site revealed that the

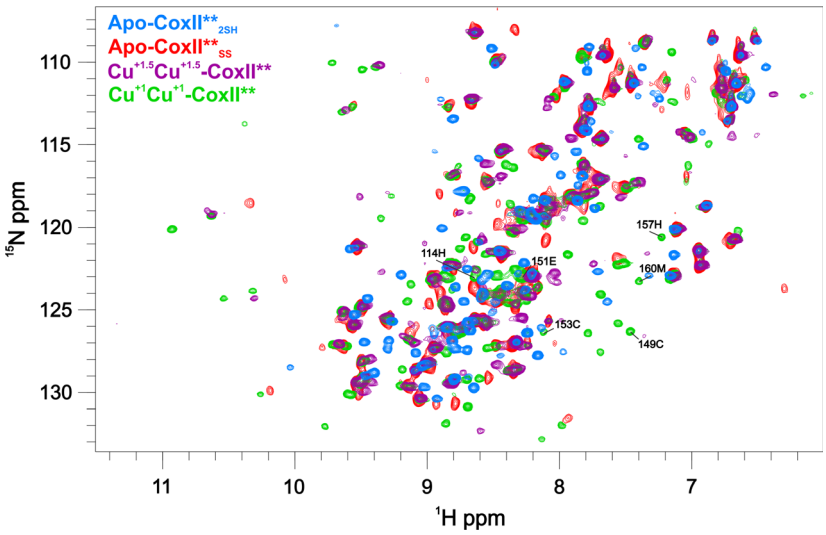

Fig. 5. Superimposed ^{15}N-^{1}H HSQC spectra of: apo- CoxII**$_{2SH}$ (light blue); apo-CoxII**$_{SS}$ (red), $Cu^{1+}Cu^{1+}$-CoxII** (green) and $Cu^{1.5+}Cu^{1.5+}$-CoxII** (purple). Protein samples were in 50 mM phosphate buffer, 200 mM NaCl, at pH 7.0. Labels indicate NH resonances from coordinating residues in $Cu^{1+}Cu^{1+}$-CoxII**.

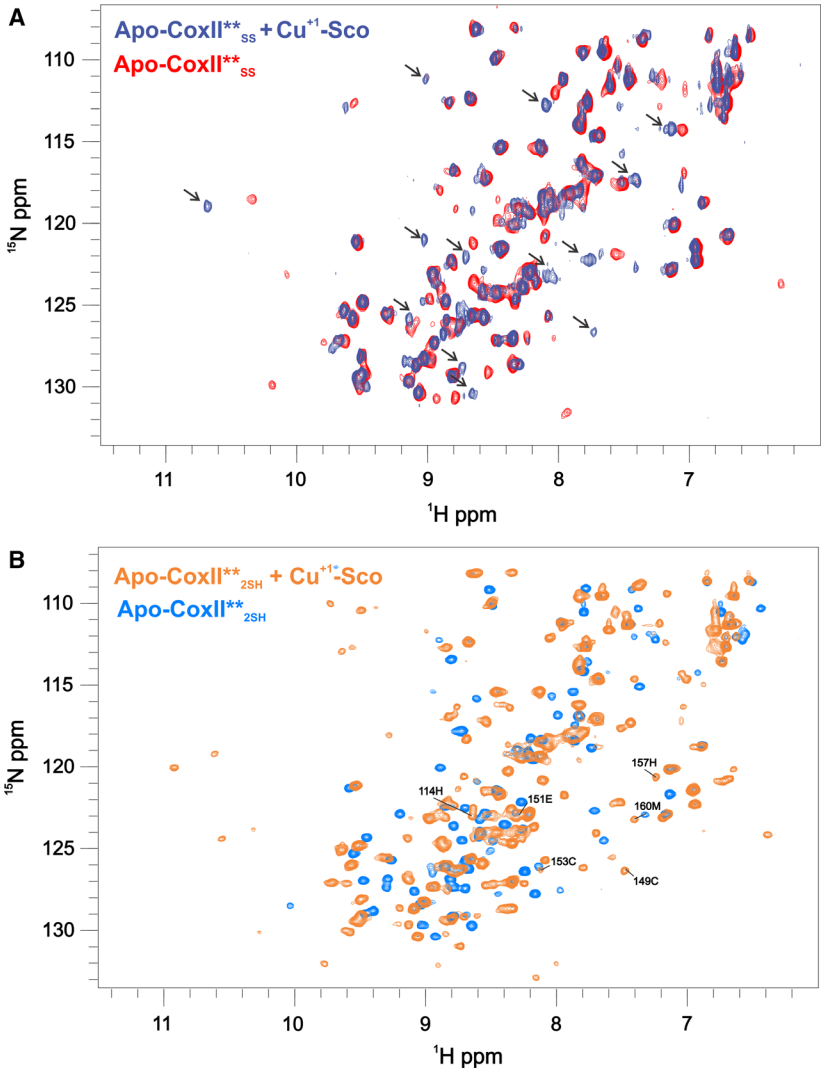

Fig. 6. (A) Superimposed ^{15}N-^{1}H HSQC spectra of: apo-CoxII**$_{SS}$ (Red); 1:1 mixture of apo-CoxII**$_{SS}$ + Cu^{+1}-Sco1 (blue). Arrows point the unidentified crosspeaks, not observed in other states of the protein (50 mM phosphate buffer, 200 mM NaCl, at pH 7.0.) (B) Superimposed ^{15}N-^{1}H HSQC spectra of: 100 μM apo-CoxII**$_{SS}$ (light blue), 100 μM apo- CoxII**$_{2SH}$ + 200 μM Cu^{+1}-Sco (orange) (50 mM phosphate buffer, 200 mm NaCl, at pH 7.0) Labels indicate the signals corresponding to the coordinating residues on Cu^{+1}Cu^{+1}-CoxII**. All spectra were recorded in 50 mM phosphate buffer, 200 mM NaCl, at pH 7.0.

reaction has proceeded to completion, with no traces of apo-CoxII**. Finally, when the reaction was exposed to oxygen, the typical purple color corresponding to the oxidized Cu_A species developed. The UV-Vis of this sample was identical to that observed for CoxII** by direct addition of metal ions in aerobic conditions (Fig. 4H).

From these data we conclude that *A. thaliana* Sco1 is a copper metallochaperone, able to insert efficiently the two copper ions into apo-CoxII**$_{2SH}$ and forming the Cu_A center.

Discussion

Sco proteins are essential players in the complex assembly process of the Cu_A site from cytochrome *c* oxidase [3,30]. The first evidence on the role of Sco proteins dates back to 1996. Glerum and coworkers reported that two Sco-like proteins could restore a copper defect in yeast [25]. A similar protein in *B. subtilis* was also shown to be essential for the assembly of the heme-copper oxidase in this organism [22]. Later, the copper-binding features of Sco proteins were described by Winge, Leary and coworkers [42]. The two essential Sco proteins in the human mitochondria were shown to perform complementary roles by Leary and Shoubridge [24,58]. Overall, genetic and physiological studies in different organisms pointed out the presence of one or two Sco-like proteins involved in this process. These studies pointed to the functional annotation of Sco proteins as metallochaperones.

Biochemical and structural evidence later expanded this diversity when the functional roles of several Sco proteins were elucidated [35–37,59]. Despite all Sco proteins bind copper, only some of them are able to insert copper ions into the Cu_A site. Here we show that Hcc1 from *A. thaliana* is a Sco protein able to deliver two copper ions into the Cu_A site of CoxII.

The crystal structure of *At*Sco1 soluble domain revealed details of the copper binding site that so far have been unclear. NMR structural analyses of human Cu-Sco1 and Cu-Sco2 pointed out histidine binding to the copper ion, but the information available from NMR of diamagnetic Cu^{+1} did not provide constraints to define the metal site geometry. Rather, the present crystal structure of *At*Sco1 disclosed the presence of a tri-coordinated copper ion, with a distorted trigonal planar coordination sphere comprising the three ligands of the conserved $CxxxCx_nH$ motif. This geometry is consistent with a Cu^{1+} ion [60] and agrees with EXAFS (Extended X-Ray Absorption Fine Structure) data for Cu^{+1}-Sco from *Saccharomyces cerevisiae* [23] and *B. subtilis* [61]. Instead, the geometry is not consistent with the expected four-coordinate, distorted tetragonal copper site expected for Cu^{+2}-Sco [44,45,61].

A crystal structure of copper-bound Sco from *B. japonicum* is available (PDB ID 4WBR), annotated as a Cu^{+2} Sco form. Indeed, this structure displays electron density compatible with a water molecule acting as a fourth ligand of the metal ion. Thus, this structure provides details for a Cu^{2+} site in Sco proteins. Instead, in our crystal structure of Cu-bound *At*Sco1, the absence of a fourth copper ligand in all molecules of the asymmetric unit, supports the presence of a tri-coordinated Cu^{+1} metal site.

A comparison of Cu^{+1} bound *At*Sco1 with Cu^{+2}-Sco from *B. japonicum* and human Ni^{+2}-Sco1 (PDB ID 2GGT) [34] reveals that the conformation of the loop containing the cysteine ligands is conserved, despite the differences in the oxidation state or the identity of the metal ion (Fig. 3). Moreover, in Ni^{+2} human Sco2 the two cysteine ligands are oxidized forming a disulfide bridge. We conclude that the geometry of the metal site is constrained by the protein scaffold, and the main difference between the Cu^{+1} and Cu^{+2} forms is the presence of a fourth ligand. Given that Sco proteins are presumed to transport and deliver Cu^{+1} *in vivo*, the distorted trigonal geometry lacking a fourth ligand may provide a higher accessibility for copper, facilitating metal transfer.

We also show that *At*Sco1 is not able to reduce the disulfide bridge of apo-$CoxII_{SS}$, in contrast to the function reported for *T. thermophilus* Sco and Cu^{1+} bound human Sco2. The presence of an intermediate state in the process of copper mediated disulfide reduction could be compared with the human case. In this system, prior interaction of CoxII with Cu^{1+}-Sco1 is required for disulfide reduction via Cu^{+1}-Sco2 and complete metallation [36]. This scenario is consistent with our findings for *At*Sco1. This protein appears to work in a similar manner as human Sco1, but the absence of a reductase blocks the Cu_A formation process and the complex is trapped in an unproductive species.

Rosato et. al. have analyzed the structural features that characterize Sco proteins from different prokaryotic organisms and proposed a general model for Sco function, based on the evolutionary relationship with peroxiredoxins and thiol/disulfide oxidoreducatases. The proposed functions for this family includes thiol/disulfide redox activity, copper mediated redox activity, and metal transfer [33]. Indeed, the first two functions have been demonstrated for Sco family members. Previous work has shown that *T. thermophilus* Sco is a thiol-reductase for Cu_A biogenesis, whereas the metallochaperone activity is provided by the soluble protein PCu_AC that does not belong to the Sco family. In human mitochondria, both functions are carried out by Cu^{+1} bound Sco proteins. The present work further highlights the functional diversity of Sco proteins and the diverse mechanisms of Cu_A assembly in different organisms, summarized in Fig. 7.

Plants express two Sco homologs that co-localize in mitochondria. González and coworkers have shown

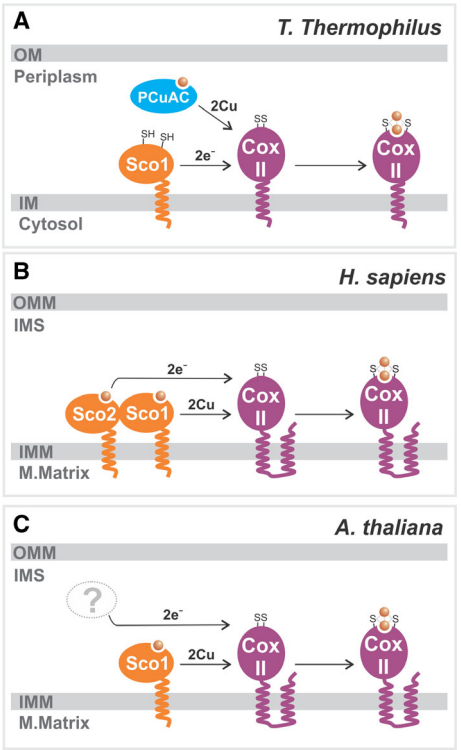

Fig. 7. Models for Cu_A biogenesis in (A) bacterial periplasm, (B) human mitochondria and (C) plant mitochondria. (OM, Outer Bacterial Membrane; IM, Inner Bacterial Membrane; OMM, Outer Mitochondrial Membrane; IMS, Inter Membrane Space; IMM, Inner Mitochondrial Membrane).

that *At*Sco1 (formerly Hcc1) is essential for CoxII function, while Hcc2, lacking metal binding residues, was not essential. Here we show that *At*Sco1 is a specific metallochaperone for CoxII, accounting for the impact of the deletion of the Sco gene in the plant phenotype [38,39].

Methods

Protein production and purification

The DNA coding for *coxII*** and *hcc1* were provided by Genescript in a pUC57 vector and then subcloned into isopropyl β-D-1-thiogalactopyranoside (IPTG) inducible vectors.

*coxII*** was cloned between the BamHI and NdeI sites in plasmid pET9a (Novagen-Merck, Darmstadt, Germany) and the protein was overproduced in *E. coli* BL21-Gold (DE3) cells (Agilent, Santa Clara, CA, USA) grown in LB or M9 media. Uniformly labelled CoxII** was produced by growing the bacterial cells in minimal M9 medium with $^{15}NH_4Cl$ and/or ^{13}C-glucose as required. The numbering scheme for CoxII** is adopted by analogy with CoxII from *Thermus thermophilus* (Fig. 4). The sequence coding for the soluble domain of Hcc1 was cloned between BamHI and NdeI sites, downstream the sequence for a histidine$_6$ tag in plasmid pET28a (Novagen-Merck). The protein was overproduced in *E. coli* BL21-Star (DE3) cells (ThermoFisher, Waltham, MA, USA), in LB medium. Cells were lysed by sonication, and subsequently centrifuged at 12 000 ***g*** for 15 min at 4 °C, to separate cell debris.

The strategy for the purification of CoxII** was based on the high thermal stability of the protein. First, DNA was precipitated from the soluble cell fraction by adding 10 mg·mL^{-1} streptomycin sulphate and separated by centrifugation at 12 000 ***g*** for 15 min at 4 °C. Then, the supernatant was incubated at 60 °C for 20 min and precipitated proteins were removed by centrifugation at 12 000 ***g*** for 15 min at 4 °C. The supernatant was treated with 303 g·L^{-1} ammonium sulphate and pelleted by centrifugation at 5000 ***g*** for 15 min at 4 °C. The pellet was resuspended and dialyzed against 50 mM phosphate buffer at pH 7.5 to eliminate the salt excess. After, the sample was loaded onto a Q-sepharose column equilibrated in the same buffer, and eluted with a 0–500 mM NaCl gradient. Fractions containing CoxII** were pooled, concentrated and loaded onto a Hi-load 16/600 Superdex 200 pg column (GE Healthcare, Uppsala, Sweden), and elution was performed with 50 mM phosphate, 200 mM NaCl, at pH 7.0.

Hcc1 was purified using a His-trap column loaded with zinc. The soluble cell fraction was loaded onto the column and the protein was eluted with a 0–300 mM gradient of imidazole in 20 mM Tris, 500 mM NaCl, at pH 7.5. The histidine$_6$ tag was cleaved by treating the sample with thrombin (1 μg per 10 mg Hcc1) during an overnight dialysis at 4 °C against 20 mM Tris, 500 mM NaCl, to remove the excess of imidazole. After, protein samples were concentrated and re-loaded onto the Hi-trap-Zn column to remove the free histidine$_6$ tag. The flow trough was concetrated an loaded onto a Hi-load 16/600 Superdex 200 pg column (GE Healthcare), and the protein was eluted with 50 mM phosphate, 200 mM NaCl, 1 mM DTT, at pH 7.0.

For the Hcc1/Sco1 construct produced in this work we use the following numbering scheme: The first four residues (^{1}GSHM^4) corresponds to the remaining residues after thrombin cleavage of histidine$_6$ tag, and residue five corresponds to the N-terminus of the soluble domain (Fig. 3).

Determination of protein and copper concentrations

Protein concentrations were determined by electronic absorption at 280 nm, using molar extintion coefficients (ε_{280} = 19 035 M^{-1}·cm^{-1} for Hcc1/Sco1 and 20 065 M^{-1}·cm^{-1} for CoxII**) estimated by the ProtParam tool (https://web.expasy.org/protparam/). Copper concentrations in protein samples were determined by complexation with the colorimetric reagents 4-(2-pyridilazo)-resorcinol (PAR) for Cu^{+2} and Bcs for Cu^{+1} under denaturing conditions (6M guanidine chloride). Both reagents were purchased from Sigma-Aldrich. Metal content in all Cu-Sco1 samples ranged between 0.9–1.00 metal/protein.

UV-Visible electronic spectra were recorded at room temperature in a Jasco 550 spectrophotometer.

All experiments were performed in 20 mM phosphate buffer, 100 mM NaCl, pH 7.0. Reduced apo-proteins were purified in the presence of 1 mM DTT, and treated with 5–10 mM DTT for 30 min to ensure complete reduction. DTT was then removed by desalting with PD MiniTrap G25 columns (GE Healthcare) in an anaerobic chamber (Coy Lab Products, Grass Lake, MI, USA).

Crystallization, data collection and structure determination

Crystallization screenings were carried out using the sitting-drop vapor diffusion method and a Gryphon (Art Robbins Instruments, Sunnyvale, CA, USA) or Mosquito (TTP Labtech, Melbourn, UK) nanoliter-dispensing crystallization robot. Following optimization, crystals of Cu^{2+}-Sco1 soluble domain grew after 15 days from a 12 mg·mL^{-1} protein solution, by mixing 1 μL of protein solution and 1 μL of mother liquor (100 mm Hepes, 23% w/v PEG 3350, 10% v/v Tacsimate, at pH 7.5), in a hanging drop setup with 1 mL mother liquor in the reservoir, at 20 °C. Single crystals were cryprotected in mother liquor containing 30% glycerol as cryoprotectant and flash-frozen in liquid nitrogen. X-ray diffraction data were collected at the synchrotron beamline MASSIF-3 (ESRF, Grenoble, France), at 100 K, using wavelength 0.9677 Å. Diffraction data were processed using XDS [62] and scaled with Aimless from the CCP4 program suite [63].

The crystal structure of *At*Sco1 soluble domain was solved by molecular replacement using the program Phaser [64] and the atomic coordinates of human Sco1 residues 135–300 from chain A in PDB ID 2GGT as search probe. The structure was refined by iterative cycles of manual model building with Coot [65] and refinement with Buster [66]. Cu^{+1} atoms were manually placed in mFo–DFc sigma-A-weighted electron density maps employing COOT and the resulting model was refined as described above. The final structure was validated through the Molprobity server (http://molprobity.biochem.duke.edu). It contained 98% of residues within favoured regions of Ramachandran plot, with no outliers. Figures were generated and rendered with PYMOL version (Schrödinger, LLC). Atomic coordinates and structure factors were deposited in the Protein Data Bank under the accession code 6N5U (PDB ID 6N5U).

Nuclear magnetic resonance

The NMR experiments were carried out on a 700-MHz Bruker Avance III spectrometer equipped with a triple resonance inverse (TXI) probe. All experiments were carried out at 298 K using standard techniques. Backbone resonance assignments for $Cu^{+1}Cu^{+1}$-CoxII** were obtained by analyzing HSQC, HNCO, HN(CA)CO, HNCA, HN(CO)CA, CBCA(CO)NH, and HNCACB experiments acquired on a uniformly labeled ^{13}C and ^{15}N sample prepared in 100 mM KCl and 100 mM potassium phosphate buffer at pH 6.0. The backbone ^{15}N and ^{1}H assignments were transferred from pH 6.0 to 7.0 by following the position of the N-H cross peaks in HSQC spectra in a pH titration. All NMR data were processed using the TopSpin™ NMR suite and analyzed using CcpNmr [67].

Protein mixtures

Protein–protein titrations were performed under anaerobic conditions using 100 μM ^{15}N-CoxII** in 50 mM potassium phosphate buffer at pH 7.0 and followed by ^{1}H,^{15}N-HSQC experiments. Samples of proteins with their cysteine thiols in the reduced state were obtained by addition of 5–10 mM DTT for 30 min followed by removal of the reducing agent through desalting by PD MiniTrap G25 columns (GE Healthcare) in an anaerobic chamber (Coy Lab Products). Cu^{+1}-bound forms of Sco proteins were obtained by addition of two equivalents of Cu^{+1} to the reduced samples followed by removal of excess Cu^{+1} through desalting in anaerobic chamber.

Acknowledgements

We thank Ahmed Haouz and Patrick Weber (Institut Pasteur) for their help with robot-driven crystallization screenings. We thank M. Avecilla for the excellent technical assistance in this work.

We acknowledge the synchrotron source in ESRF (Grenoble, France) for granting access to their facilities, and their staff members for the helpful assistance. We acknowledge funding from the grant PICT 2012-1285, from the Agencia Nacional de Promoción Científica y Tecnológica (ANPCyT, Argentina). MNL and AJV are staff members of the Consejo Nacional de Investigaciones Científicas y Técnicas (CONICET, Argentina). MEL, MM and EG are recipient of fellowships from CONICET. The NMR spectrometer was supported with grants from ANPCyT. We also thank support from the Argentina-France ECOS exchange program (ECOS A15B01) to AJV and PMA.

Conflict of interest

The authors declare no conflict of interest.

Author contributions

MEL performed protein expression/purification, biochemical and spectroscopic studies. EG, MNL and PA crystallized and solved the structure of Sco1. MEL, MNM and AJV designed the experiments and wrote the paper. All authors revised the manuscript and contributed to the final text.

References

1 Wikström M, Krab K & Sharma V (2018) Oxygen activation and energy conservation by cytochrome c Oxidase. *Chem Rev* **118**, 2469–2490.
2 Timón-Gómez A, Nývltová E, Abriata LA, Vila AJ, Hosler J & Barrientos A (2018) Mitochondrial cytochrome c oxidase biogenesis: recent developments. *Semin Cell Dev Biol* **76**, 163–178.
3 Jett KA & Leary SC (2018) Building the CuA site of cytochrome c oxidase: a complicated, redox-dependent process driven by a surprisingly large complement of accessory proteins. *J Biol Chem* **293**, 4644–4652.
4 Leary SC (2010) Redox regulation of SCO protein function: controlling copper at a mitochondrial crossroad. *Antioxid Redox Signal* **13**, 1403–1416.
5 Festa RA & Thiele DJ (2011) Copper: an essential metal in biology. *Curr Biol* **21**, R877–R883.
6 Scheiber I, Dringen R & Mercer JFB (2013) Copper: Effects of Deficiency and Overload. In Metal Ions in Life Sciences, p. 573. Springer Science + Business Media, Dordrecht.
7 Robinett NG, Culbertson EM, Peterson RL, Sanchez H, Andes DR, Nett JE & Culotta VC (2019) Exploiting the vulnerable active site of a copper-only superoxide dismutase to disrupt fungal pathogenesis. *J Biol Chem* **294**, 2700–2713.

8 Peter Guengerich F (2018) Thematic Minireview Series: metals in biology 2018. *J Biol Chem* **293**, 4603.
9 Macomber L & Imlay JA (2009) The iron-sulfur clusters of dehydratases are primary intracellular targets of copper toxicity. *Proc Natl Acad Sci USA* **106**, 8344–8349.
10 Foster AW, Osman D & Robinson NJ (2014) Metal preferences and metallation. *J Biol Chem* **289**, 28095–28103.
11 Bertini I, Cavallaro G & McGreevy KS (2010) Cellular copper management-a draft user's guide. *Coord Chem Rev* **254**, 506–524.
12 Ma Z, Jacobsen FE & Giedroc DP (2009) Coordination chemistry of bacterial metal transport and sensing. *Chem Rev* **109**, 4644–4681.
13 Dennison C, David S & Lee J (2018) Bacterial copper storage proteins. *J Biol Chem* **293**, 4616–4627.
14 Kenney GE & Rosenzweig AC (2018) Methanobactins: Maintaining copper homeostasis in methanotrophs and beyond. *J Biol Chem* **293**, 4606–4615.
15 Argüello JM, Raimunda D & González-Guerrero M (2012) Metal transport across biomembranes : emerging models for a distinct chemistry. *J Biol Chem* **287**, 13510–13517.
16 O'Halloran TV & Culotta VC (2000) Metallochaperones, an intracellular shuttle service for metal ions. *J Biol Chem* **275**, 25057–25060.
17 Rae TD, Schmidt PJ, Pufahl RA, Culotta VC & O'Halloran TV (1999) Undetectable intracellular free copper: the requirement of a copper chaperone for superoxide dismutase. *Science* **284**, 805–808.
18 Robinson NJ & Winge DR (2010) Copper Metallochaperones. *Annu Rev Biochem* **79**, 537–562.
19 Kroneck PMH (2018) Walking the seven lines: binuclear copper A in cytochrome c oxidase and nitrous oxide reductase. *J Biol Inorg Chem* **23**, 27–39.
20 Gamelin DR, Randall DW, Hay MT, Houser RP, Mulder TC, Canters GW, De Vries S, Tolman WB, Lu Y & Solomon EI (1998) Spectroscopy of mixed-valence Cu(A)-type centers: Ligand-field control of ground-state properties related to electron transfer. *J Am Chem Soc* **120**, 5246–5263.
21 Ross MO, Fisher OS, Morgada MN, Krzyaniak MD, Wasielewski MR, Vila AJ, Hoffman BM & Rosenzweig AC (2019) Formation and electronic structure of an atypical CuA site. *J Am Chem Soc* **141**, 4678–4686.
22 Mattatall NR, Jazairi J & Hill BC (2000) Characterization of ypmQ, an accessory protein required for the expression of cytochrome c oxidase in *Bacillus subtilis*. *J Biol Chem* **275**, 28802–28809.
23 Nittis T, George GN & Winge DR (2001) Yeast Sco1, a protein essential for cytochrome c oxidase function Is a Cu (I)-binding protein. *Biochemistry* **276**, 42520–42526.
24 Leary SC, Kaufman BA, Pellecchia G, Guercin GH, Mattman A, Jaksch M & Shoubridge EA (2004) Human SCO1 and SCO2 have independent, cooperative functions in copper delivery to cytochrome c oxidase. *Hum Mol Genet* **13**, 1839–1848.
25 Glerum DM, Shtanko A & Tzagoloff A (1996) Characterization of C O X 1 7, a yeast gene involved in copper metabolism and assembly of cytochrome oxidase. *J Biol Chem* **24**, 14504–14509.
26 Letts JA, Fiedorczuk K & Sazanov LA (2016) The architecture of respiratory supercomplexes. *Nature* **537**, 644–648.
27 Guo R, Zong S, Wu M, Gu J & Yang M (2017) Architecture of human mitochondrial respiratory megacomplex I2III2IV2. *Cell* **170**, 1247–1257.e12.
28 Hartley AM, Lukoyanova N, Zhang Y, Cabrera-Orefice A, Arnold S, Meunier B, Pinotsis N & Maréchal A (2018) Structure of yeast cytochrome c oxidase in a supercomplex with cytochrome bc1. *Nat Struct Mol Biol* **26**, 78–83.
29 Williams PA, Blackburn NJ, Sanders D, Bellamy H, Stura EA, Fee JA & McRee DE (1999) The CuA domain of *Thermus thermophilus* ba3-type cytochrome c oxidase at 1.6 A resolution. *Nat Struct Biol* **6**, 509–516.
30 Banci L, Bertini I, Cavallaro G & Ciofi-Baffoni S (2011) Seeking the determinants of the elusive functions of Sco proteins. *FEBS J* **278**, 2244–2262.
31 Rigby K, Cobine PA, Khalimonchuk O & Winge DR (2008) Mapping the functional interaction of Sco1 and Cox2 in cytochrome oxidase biogenesis. *J Biol Chem* **283**, 15015–15022.
32 Balatri E, Banci L, Bertini I, Cantini F & Ciofi-Baffoni S (2003) Solution structure of Sco1: A thioredoxin-like protein involved in cytochrome c oxidase assembly. *Structure* **11**, 1431–1443.
33 Banci L, Bertini I, Cavallaro G & Rosato A (2007) The functions of Sco proteins from genome-based analysis. *J Proteome Res* **6**, 1568–1579.
34 Banci L, Bertini I, Calderone V, Ciofi-Baffoni S, Mangani S, Martinelli M, Palumaa P & Wang S (2006) A hint for the function of human Sco1 from different structures. *Proc Natl Acad Sci USA* **103**, 8595–8600.
35 Abriata LA, Banci L, Bertini I, Ciofi-Baffoni S, Gkazonis P, Spyroulias GA, Vila AJ & Wang S (2008) Mechanism of CuA assembly. *Nat Chem Biol* **4**, 599–601.
36 Morgada MN, Abriata LA, Cefaro C, Gajda K, Banci L & Vila AJ (2015) Loop recognition and copper-mediated disulfide reduction underpin metal site assembly of Cu $_A$ in human cytochrome oxidase. *Proc Natl Acad Sci USA* **112**, 11771–11776.
37 Abicht HK, Schärer MA, Quade N, Ledermann R, Mohorko E, Capitani G, Hennecke H & Glockshuber R (2014) How periplasmic thioredoxin TlpA reduces bacterial copper chaperone ScoI and cytochrome oxidase subunit II (CoxB) prior to metallation. *J Biol Chem* **289**, 32431–32444.
38 Attallah CV, Welchen E, Martin AP, Spinelli SV, Bonnard G, Palatnik JF & Gonzalez DH (2011) Plants

contain two SCO proteins that are differentially involved in cytochrome c oxidase function and copper and redox homeostasis. *J Exp Bot* **62**, 4281–4294.
39 Steinebrunner I, Gey U, Andres M, Garcia L & Gonzalez DH (2014) Divergent functions of the Arabidopsis mitochondrial SCO proteins: HCC1 is essential for COX activity while HCC2 is involved in the UV-B stress response. *Front Plant Sci* **5**, 1–17.
40 Steinebrunner I, Landschreiber M, Krause-Buchholz U, Teichmann J & Rödel G (2011) HCC1, the Arabidopsis homologue of the yeast mitochondrial copper chaperone SCO1, is essential for embryonic development. *J Exp Bot* **62**, 319–330.
41 Ye Q, Imriskova-Sosova I, Hill BC & Jia Z (2005) Identification of a disulfide switch in BsSco, a member of the Sco family of cytochrome c oxidase assembly proteins. *Biochemistry* **44**, 2934–2942.
42 Horng YC, Leary SC, Cobine PA, Young FBJ, George GN, Shoubridge EA & Winge DR (2005) Human Sco1 and Sco2 function as copper-binding proteins. *J Biol Chem* **280**, 34113–34122.
43 Imriskova-Sosova I, Andrews D, Yam K, Davidson D, Yachnin B & Hill BC (2005) Characterization of the redox and metal binding activity of BsSco, a protein implicated in the assembly of cytochrome c oxidase. *Biochemistry* **44**, 16949–16956.
44 Basumallick L, Sarangi R, DeBeer George S, Elmore B, Hooper AB, Hedman B, Hodgson KO & Solomon EI (2005) Spectroscopic and density functional studies of the red copper site in nitrosocyanin: role of the protein in determining active site geometric and electronic structure. *J Am Chem Soc* **127**, 3531–3544.
45 Siluvai GS, Mayfield M, Nilges MJ, Debeer George S & Blackburn NJ (2010) Anatomy of a red copper center: Spectroscopic identification and reactivity of the copper centers of *Bacillus subtilis* Sco and its Cys-to-ala variants. *J Am Chem Soc* **132**, 5215–5226.
46 Abajian C & Rosenzweig AC (2006) Crystal structure of yeast Sco1. *J Biol Inorg Chem* **11**, 459–466.
47 Garman EF & Nave C (2009) Radiation damage in protein crystals examined under various conditions by different methods. *J Synchrotron Radiat* **16**, 129–132.
48 Yang J, Regier T, Dynes JJ, Wang J, Shi J, Peak D, Zhao Y, Hu T, Chen Y & Tse JS (2011) Soft X-ray induced photoreduction of organic Cu(II) compounds probed by X-ray absorption near-edge (XANES) spectroscopy. *Anal Chem* **83**, 7856–7862.
49 Blackburn NJ, Barr ME, Woodruff WH, van der Ooost J & de Vries S (1994) Metal-metal bonding in biology: EXAFS evidence for a 2.5 Å copper-copper BOND in the CUA center of cytochrome oxidase. *Biochemistry* **33**, 10401–10407.
50 Iwata S, Ostermeier C, Ludwig B & Michel H (1995) Structure at 2.8 Å resolution of cytochrome c oxidase from Paracoccus denitrificans. *Nature* **376**, 660–669.
51 Slutter CE, Sanders D, Wittung P, Malmström BG, Aasa R, Richards JH, Gray HB & Fee JA (1996) Water-soluble, recombinant CuA-domain of the cytochrome ba3 subunit II from *Thermus thermophilus*. *Biochemistry* **35**, 3387–3395.
52 Lu Y (2003) Electron Transfer: Cupredoxins. Comprehensive Coordination Chemistry II, 2nd edn., pp. 91–122. Pergamon, Oxford.
53 Rathore S, Berndtsson J, Marin-Buera L, Conrad J, Carroni M, Brzezinski P & Ott M (2019) Cryo-EM structure of the yeast respiratory supercomplex. *Nat Struct Mol Biol* **26**, 50–57.
54 Zaballa M-E, Abriata LA, Donaire A & Vila AJ (2012) Flexibility of the metal-binding region in apo-cupredoxins. *Proc Natl Acad Sci USA* **109**, 9254–9259.
55 Morgada MN, Abriata LA, Zitare U, Alvarez-Paggi D, Murgida DH & Vila AJ (2014) Control of the electronic ground state on an electron-transfer copper site by second-sphere perturbations. *Angew Chemie – Int Ed* **53**, 6188–6192.
56 Abriata LA, Vila AJ, Dal Peraro M & Peraro MD (2014) Molecular dynamics simulations of apocupredoxins: insights into the formation and stabilization of copper sites under entatic control. *J Biol Inorg Chem* **19**, 565–575.
57 Lopez LC, Mukhitov N, Handley LD, Hamme CS, Hofman CR, Euers L, McKinney JR, Piers AD, Wadler E & Hunsicker-Wang LM (2018) Characterization and effect of metal ions on the formation of the *Thermus thermophilus* Sco mixed disulfide intermediate. *Protein Sci* **27**, 1942–1954.
58 Leary SC, Cobine PA, Kaufman BA, Guercin GH, Mattman A, Palaty J, Lockitch G, Winge DR, Rustin P, Horvath R *et al.* (2007) The human cytochrome c oxidase assembly factors SCO1 and SCO2 have regulatory roles in the maintenance of cellular copper homeostasis. *Cell Metab* **5**, 9–20.
59 Siluvai GS, Nakano MM, Mayfield M, Nilges MJ & Blackburn NJ (2009) H135A controls the redox activity of the Sco copper center. Kinetic and spectroscopic studies of the His135Ala variant of *Bacillus subtilis* Sco. *Biochemistry* **48**, 12133–12144.
60 Balamurugan R, Palaniandavar M & Srinivasa Gopalan R (2001) Trigonal planar copper(I) complex: Synthesis, structure, and spectra of a redox pair of novel copper(II/I) complexes of tridentate bis (benzimidazol-2′-yl) ligand framework as models for electron-transfer copper proteins. *Inorg Chem* **40**, 2246–2255.
61 Andruzzi L, Nakano M, Nilges MJ & Blackburn NJ (2005) Spectroscopic studies of metal binding and metal selectivity in Bacillus subtilis BSco, a homologue of the yeast mitochondrial protein Sco1p. *J Am Chem Soc* **127**, 16548–16558.

62 Kabsch W (2010) XDS. *Acta Crystallogr D* **66**, 125–132.
63 Winn MD, Ballard CC, Cowtan KD, Dodson EJ, Emsley P, Evans PR, Keegan RM, Krissinel EB, Leslie AGW, McCoy A *et al*. (2011) Overview of the CCP4 suite and current developments. *Acta Crystallogr D* **67**, 235–242.
64 Adams PD, Afonine PV, Bunkóczi G, Chen VB, Davis IW, Echols N, Headd JJ, Hung L-W, Kapral GJ, Grosse-Kunstleve RW *et al*. (2010) PHENIX: a comprehensive Python-based system for macromolecular structure solution. *Acta Crystallogr D* **66**, 213–221.
65 Emsley P, Lohkamp B, Scott WG & Cowtan K (2010) Features and development of COOT. *Acta Crystallogr D* **66**, 486–501.
66 Bricogne G, Blanc E, Brandl M, Flensburg C, Keller P, Paciorek W, Roversi P, Sharff A, Smart OS, Vonrhein C *et al*. (2016) BUSTER Version X.Y.Z. Glob. Phasing Ltd, Cambridge, UK.
67 Vranken WF, Boucher W, Stevens TJ, Fogh RH, Pajon A, Llinas M, Ulrich EL, Markley JL, Ionides J & Laue ED (2005) The CCPN data model for NMR spectroscopy: development of a software pipeline. *Proteins* **59**, 687–696.